



## Solution Combustion Synthesis of Iron Oxyborate ( $\text{Fe}_3\text{BO}_6$ )

Demet Ozer\* and Okan Icten 

The University of Hacettepe, Faculty of Science, Department of Chemistry, 06590, Ankara, Turkey

**Abstract:** In this study, iron oxyborate ( $\text{Fe}_3\text{BO}_6$ ) was synthesized through the solution combustion method as a potential anode material for lithium-ion batteries. Urea, glycine, citric acid, carbonyldiurea, hexamethylene tetramine, and starch were used as fuel sources and the effects of the fuels were investigated. The obtained materials were structurally characterized by FT-IR, powder-XRD, solid UV-Vis, TGA and VSM. The pure crystalline  $\text{Fe}_3\text{BO}_6$  was synthesized at low temperature and short reaction time using glycine-assisted solution combustion method. It was thermally stable up to 945 °C with a non-uniform morphology and a highly porous structure. The magnetic properties were also studied and  $\text{Fe}_3\text{BO}_6$  shows antiferromagnetic behavior.

**Keywords:**  $\text{Fe}_3\text{BO}_6$ , solution combustion synthesis, fuel effect, antiferromagnetism.

**Submitted:** December 21, 2018. **Accepted:** January 09, 2019.

**Cite this:** Ozer D, Icten O. Solution Combustion Synthesis of Iron Oxyborate ( $\text{Fe}_3\text{BO}_6$ ). JOTCSA. 2019;6(2):95-102.

**DOI:** <https://dx.doi.org/10.18596/jotcsa.500355>.

\*Corresponding author. E-mail: [demetbaykan@hacettepe.edu.tr](mailto:demetbaykan@hacettepe.edu.tr).

### INTRODUCTION

Iron oxyborate ( $\text{Fe}_3\text{BO}_6$ ) has been used in ceramics (1), drugs, pigments, gas sensors, catalysts (2), electrodes and biological probes because of magnetic (3, 4), dielectric (5), conductivity (6), optical (7), structural (8), electrochemical (9) and surface properties. It is a promising anode material in lithium-ion batteries with high reversible capacity (10), unremarkable toxicity and low cost and it is also used in sodium ion batteries with high activity (11). Up until now, different synthetic methods have been utilized to synthesize iron oxyborate. Shi and coworkers used the rheological phase reaction method and obtained the nanospherical iron oxyborate using  $\text{FeC}_2\text{O}_4 \cdot 2\text{H}_2\text{O}$  and  $\text{H}_3\text{BO}_3$  precursors at 800 °C for 5 h and at 900 °C for 3 h (12). The norbergite structure of  $\text{Fe}_3\text{BO}_6$  was prepared solid state reaction with the  $\text{Fe}_2\text{O}_3$ - $\text{H}_3\text{BO}_3$  mixture at 880 °C for 2 days (10) and  $\text{Fe}_2(\text{SO}_4)_3 \cdot \text{H}_2\text{O}$ - $\text{H}_3\text{BO}_3$  mixture at 900 °C for 9h (2). The nanocrystalline  $\text{Fe}_3\text{BO}_6$  was synthesized through the co-pyrolysis method using  $\text{FeC}_{10}\text{H}_{10}$ - $\text{H}_3\text{BO}_3$  at 700 °C for 15h in a stainless-steel autoclave (13). Starting from  $\text{Fe}_2\text{O}_3$ ,  $\text{B}_2\text{O}_3$  and HCl as a gaseous solvent,  $\text{Fe}_3\text{BO}_6$  was synthesized by vapor phase reaction and the reaction temperature was determined as higher

than 800 °C to prevent the formation of  $\text{FeBO}_3$  and lower than 905 °C, the incongruent melting point of  $\text{Fe}_3\text{BO}_6$  (14). Kumari prepared the  $\text{Fe}_3\text{BO}_6$  nanoplates via microwave assisted self-combustion method using camphor ( $\text{C}_{10}\text{H}_{16}\text{O}$ ) as a fuel with a mixture of  $\text{Fe}_2\text{O}_3$ - $\text{H}_3\text{BO}_3$  (15) and the self-controlled  $\text{Fe}_3\text{BO}_6$  growth of nanorods from a supercooled liquid precursor ( $\text{Fe}_2\text{O}_3$ - $\text{B}_2\text{O}_3$ ) (16). All these synthetic methods need long annealing time and high reaction temperature, so the agglomeration and high energy consumption problems can occur. In the last years, solution combustion method, which is time- and energy-saving method, have gained great attention (17). This method depends on the exothermic redox reaction between metal nitrate (oxidizer) and an appropriate organic fuel (reducing agent) (18). The fuel type, quantity of fuel and composition are the most important parameters affecting the obtained products. Urea, carbonyldiurea, oxalic dihydrazide, and glycine have been the most commonly used fuels because they are easy to gasify and are cheap (19). Besides, polymeric materials like maleic acid, citric acid, ethylene glycol, and polyvinyl alcohol have also been used as fuels. This technique was mostly used for

borate synthesis using different fuels. The  $\text{Li}_2\text{B}_4\text{O}_7$  (20),  $\text{LiAl}_7\text{B}_4\text{O}_{17}$  (21),  $\text{NaMgBO}_3$  (22),  $\text{SrB}_4\text{O}_7$  (23) and  $\text{YBO}_3$  (24) were synthesized using urea. The  $\text{Mg}_2\text{B}_2\text{O}_5$  was prepared using both glycine and carbohydrazide (25). citric acid was used for  $\text{LiFeBO}_3$  (26).

In this study, iron oxyborate was first synthesized by solution combustion method using  $\text{Fe}(\text{NO}_3)_3 \cdot 9\text{H}_2\text{O} - \text{H}_3\text{BO}_3$  by adjusting the fuel types and reaction temperatures. Urea, glycine, citric acid, carbohydrazide, and oxalyl dihydrazide were chosen as fuels. The obtained products were characterized by Fourier transform infrared spectroscopy (FT-IR), powder X-ray diffraction (p-XRD). Glycine was found as an appropriate fuel to obtain pure crystalline  $\text{Fe}_3\text{BO}_6$ . Thermal, surface and magnetic properties were also investigated by different techniques. It was prepared as a promising anode material with thermal stability and antiferromagnetic behavior.

## EXPERIMENTAL SECTION

### Materials

Iron(III)nitrate nonahydrate ( $\text{Fe}(\text{NO}_3)_3 \cdot 9\text{H}_2\text{O}$ , Merck), boric acid ( $\text{H}_3\text{BO}_3$ , Riedel), glycine ( $\text{C}_2\text{H}_5\text{NO}_2$ , Merck), citric acid monohydrate ( $\text{C}_6\text{H}_8\text{O}_7 \cdot \text{H}_2\text{O}$ , Merck), starch ( $\text{C}_6\text{H}_{10}\text{O}_5$ , Riedel), hexamethylene tetramine ( $\text{C}_6\text{H}_{12}\text{N}_4$ , Sigma), urea ( $\text{CH}_4\text{N}_2\text{O}$  Fischer), and carbohydrazide ( $\text{CO}(\text{NHNH}_2)_2$ , Aldrich) were of analytical grade and used without further purification.

### Synthesis

1 mmol  $\text{Fe}(\text{NO}_3)_3 \cdot 9\text{H}_2\text{O}$  was dissolved in deionized water. The amount of fuels was calculated according to the propellant chemistry (27).  $\text{Fe}(\text{NO}_3)_3 \cdot 9\text{H}_2\text{O}$  has an oxidizing power of -15. Urea (U), glycine (G), hexamethylenetetramine (HMTA), carbohydrazide (CH), citric acid (CA) and starch (S) are reducing fuels with the reducing power of +6, +9, +36, +8, +18 and +24,

respectively (18). An appropriate amount of fuel and 1 mmol boric acid were added to the iron solution. The mixture was continuously stirred up to dehydration at 90 °C. The dehydrated mixture was put in a preheated furnace at 500 °C until all combustion gases evaporated. The products were calcined at 600 °C to remove excess carbon residues.

### Characterizations

Fourier transform infrared spectra (FTIR) were applied on a Thermo-Scientific instrument using the KBr pellet method from 4000 to 400  $\text{cm}^{-1}$ . The thermal behavior of the products was examined with a Shimadzu DTG-60H thermal analyzer. The TGA and DTA curves were studied under  $\text{N}_2$  atmosphere over the interval 25-1000 °C at a heating rate of 10 °C/min. The solid UV-Vis analyses were performed by a Shimadzu UV-Vis spectrophotometer. The phase identification of products was investigated by an X-ray diffractometer (Rigaku DMAX-2200) with Cu K $\alpha$  radiation. The morphology of the powder was investigated by SEM using Quanta 200 FEG scanning electron microscopy. Magnetic measurements were performed with a Physical Properties Measurement System (PPMS).

## RESULTS AND DISCUSSIONS

For the structural analyses of  $\text{Fe}_3\text{BO}_6$ , the FT-IR spectra were recorded. The two bands at 1035  $\text{cm}^{-1}$  and 875  $\text{cm}^{-1}$  were ascribed to the B-O stretching vibration in a tetrahedral group  $\text{BO}_4$ . The trigonal  $\text{BO}_3$  group bands (B-O stretching) were seen at 1215 and 1425  $\text{cm}^{-1}$ . At 680  $\text{cm}^{-1}$  band, the B-O-B bending was shown and connected the  $\text{BO}_3$  to  $\text{FeO}_6$  groups (16). The 500-600  $\text{cm}^{-1}$  band was Fe-O stretching vibrations. When starch was used as a fuel in the synthesis process, the reaction was not completed and the  $\text{Fe}_3\text{BO}_6$  did not form due to possessing the high combustion temperature.

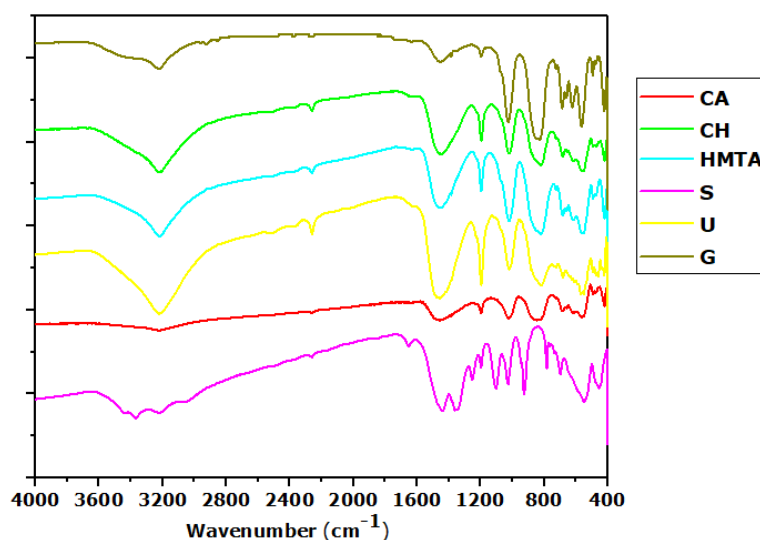


**Figure 1:** FT-IR spectra of samples synthesized by different fuels.

The p-XRD patterns of the samples were shown in Figure 2. As the starch was used as fuel, iron

oxyborate was not synthesized similar to results obtained by FT-IR. As a result of rapid

combustion, starch did not react with boric acid and  $\text{Fe}_2\text{O}_3$  was formed as a last product in the reaction medium. Therefore, reflections of sample synthesized by starch shown in a yellow pattern matched with reference hematite- $\text{Fe}_2\text{O}_3$  (JCPDS: 33-0664). On the contrary, when citric acid, carbohydrazide, glycine, hexamethylene tetramine, and urea were utilized as fuel sources, the characteristic diffraction peaks of  $\text{Fe}_3\text{BO}_6$  were observed as seen in Figure 2 and p-XRD patterns

were compatible with the reference  $\text{Fe}_3\text{BO}_6$  (JCPDS:70-0880) (28). They were an orthorhombic structure with Pnma space group (11). The unreacted  $\text{B}_2\text{O}_3$  peak at  $2\theta=28$  was shown in the samples which citric acid, carbohydrazide, hexamethylene tetramine, and urea were utilized as a fuel. No impurity phases were detected when glycine was used as a fuel.

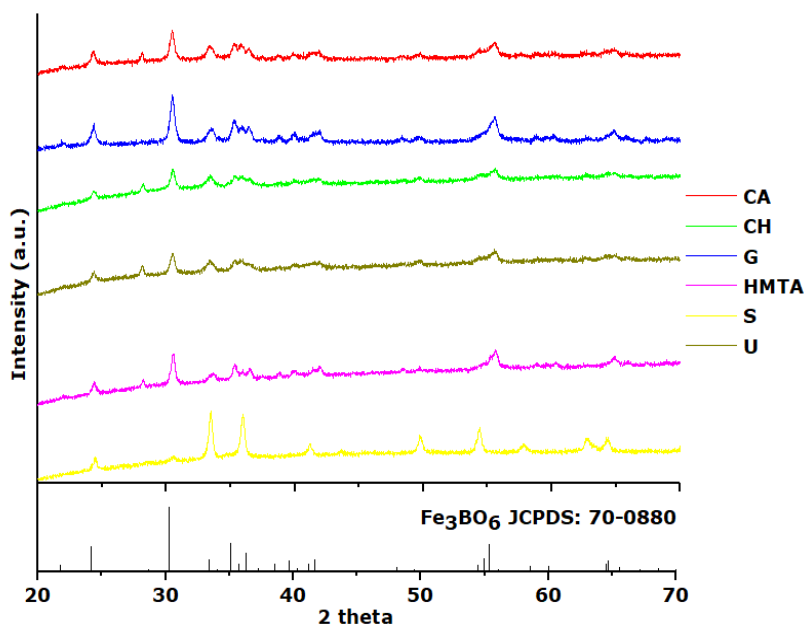


**Figure 2:** Powder XRD patterns of samples synthesized by different fuels.

The solid UV-Vis spectrum of  $\text{Fe}_3\text{BO}_6$  in the 200-900 nm region was shown in Figure 3. The ligand-metal charge transition was found at 220 nm. The broad band between 400-500 nm indicated the ligand field transition  ${}^6\text{A}_1\text{-}{}^4\text{T}_1$  of the  $3d^5$  electrons in the Fe ions (7).

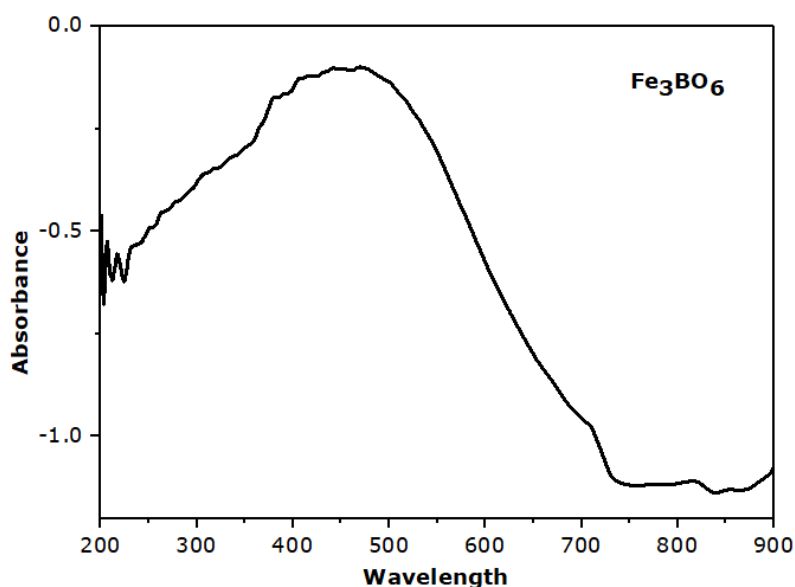


**Figure 3.** The solid UV-Vis spectrum of glycine-assisted synthesized  $\text{Fe}_3\text{BO}_6$ .

The thermal behavior of  $\text{Fe}_3\text{BO}_6$  was investigated and TGA/DTA curves were shown in Figure 4. The first weight loss of about 2.3 % occurred from room temperature to 200 °C due to the loss of adsorbed water and unreacted boric acid. The

second weight loss about 0.8 % appeared within 550-630 °C because of phase transition and a small amount of  $\text{Fe}_3\text{BO}_6$  turns amorphous phase to crystalline phase. After 945 °C,  $\text{Fe}_3\text{BO}_6$  started to decompose to  $\text{Fe}_2\text{O}_3$  and  $\text{B}_2\text{O}_3$  (12).

Considering thermal analysis results, it can be said that the product is thermally stable up to 945 °C.

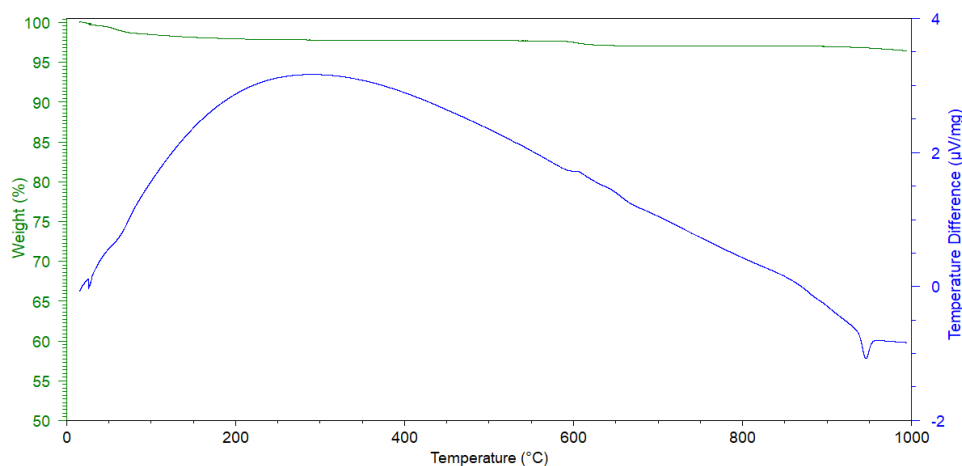


**Figure 4.** TG/DT analysis of glycine assisted synthesized  $\text{Fe}_3\text{BO}_6$

The morphology of glycine-assisted synthesized  $\text{Fe}_3\text{BO}_6$  was shown in Figure 5. As seen in the SEM images,  $\text{Fe}_3\text{BO}_6$  has a non-uniform morphology and a highly porous structure with variable pore sizes. These pores can be effective for the transport of lithium ions in Li-ion batteries.

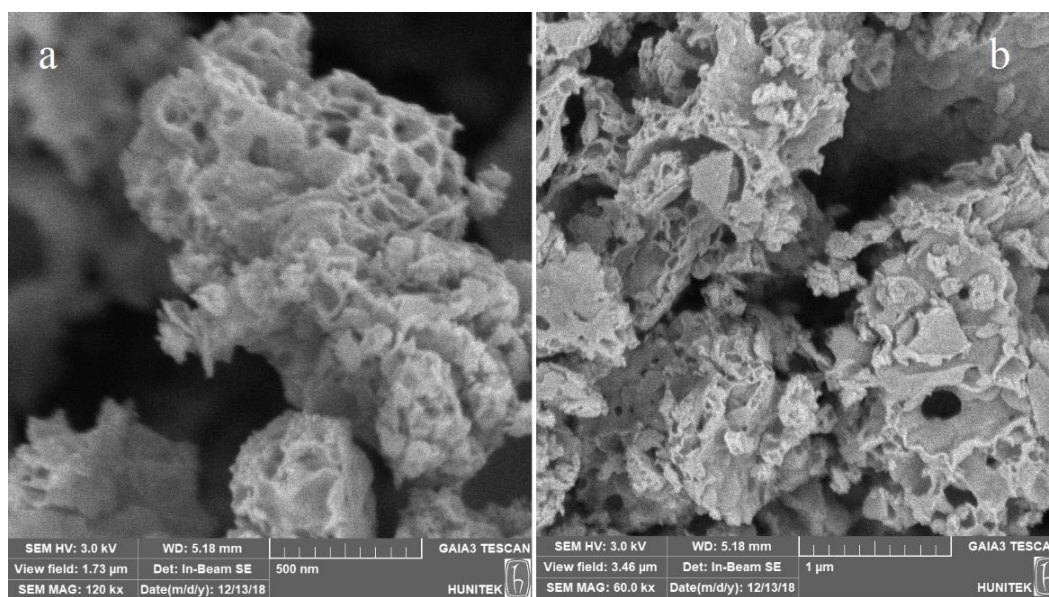


**Figure 5.** SEM images of glycine-assisted synthesized  $\text{Fe}_3\text{BO}_6$ .

The magnetization curves of glycine-assisted  $\text{Fe}_3\text{BO}_6$  from 25 °C to -268°C were given in Figure 6. At room temperature, the sample has soft antiferromagnetic behavior due to an observed low resistivity (the small area of hysteresis loop), coercivity ( $H_c=6.6$  Oe) and residual magnetism ( $B_r=0.09$  emu/g). However, when temperature

decreased from 25 °C to -268°C during magnetization analysis, its magnetic property changed as a hard antiferromagnetic behavior depending on the increase of the area of the hysteresis curve and coercivity ( $H_c=752$  Oe), residual magnetism ( $B_r=4.7$  emu/g) compared to analysis of room temperature (29).

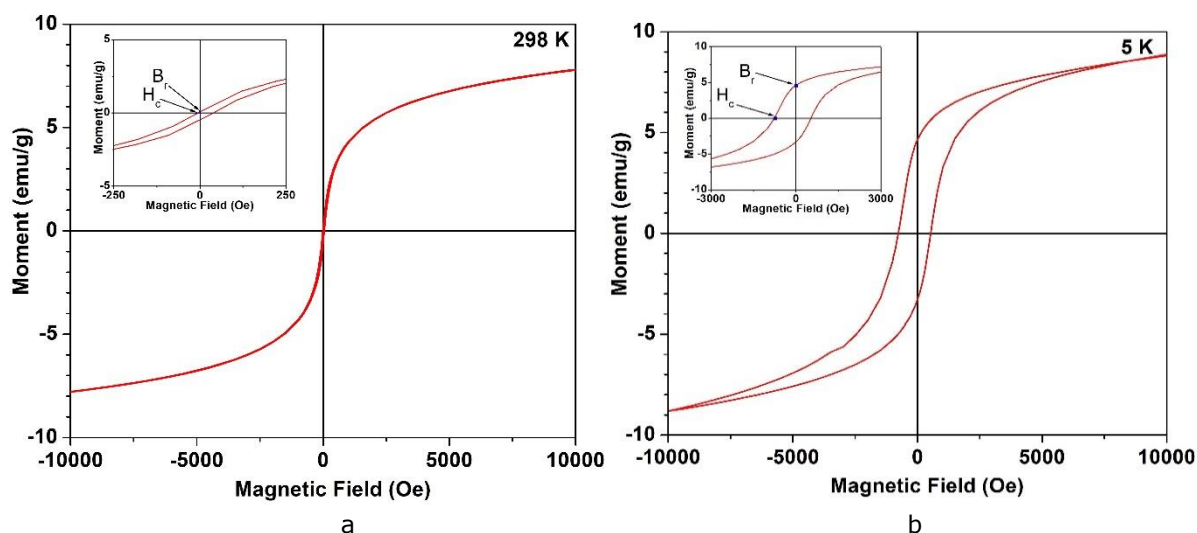


**Figure 6.** Magnetization curves of glycine assisted synthesized  $\text{Fe}_3\text{BO}_6$  (a) 25 °C (room temperature) (b)-268 °C.

## CONCLUSIONS

This study proved that  $\text{Fe}_3\text{BO}_6$  could successfully be synthesized via solution combustion method assisted glycine as a fuel. All characteristic peaks belonging to the  $\text{Fe}_3\text{BO}_6$  structure were seen in FT-IR spectra except for one sample that starch was utilized as a fuel. A similar result was obtained from XRD analysis. TGA results showed that  $\text{Fe}_3\text{BO}_6$  was quite stable up to 945 °C. The solid UV-Vis spectrum of the sample synthesized by using glycine demonstrated a broad-band at 400-500 nm due to ligand field transition. Additionally, it was seen that  $\text{Fe}_3\text{BO}_6$  possessed a highly porous network structure with non-uniform morphology and showed soft and hard antiferromagnetic behavior at 25 °C and -268 °C, respectively. The results from this study indicate that  $\text{Fe}_3\text{BO}_6$  synthesized by using glycine can be used as potential anode material for lithium-ion batteries.

## REFERENCES

1. Ram S, Kumari K, Kotnala R. Synthesis of norbergite  $\text{Fe}_3\text{BO}_6$  of single crystallites from a borate glass. *Transactions of the Indian Ceramic Society*. 2010;69(3):165-70.
2. Meydan E, Öztürk ÖF. Synthesis, Characterization, Magnetic Properties and Catalytic Performance of Iron Orthoborate. *Asian Journal of Chemistry*. 2016;28(6).
3. Buchelnikov V, Danchin N, Dolgushin D, Isotov A, Shavrov V, Tsymbal L, et al. The magnetoacoustic anomaly in  $\text{Fe}_3\text{BO}_6$ . *Journal of magnetism and magnetic materials*. 2004;272:2113-4.
4. Tsymbal L, Bazaliy YB, Bezmaternykh L, Slawska-Waniewska A, Vasiliev S, Nedelko N, et al. Orientation phase transition in  $\text{Fe}_3\text{BO}_6$ : Experimental determination of the order of the transition. *Physical Review B*. 2006;74(13):134429.
5. Kumari K. Magnetic and dielectric properties of  $\text{Fe}_3\text{BO}_6$  nanoplates prepared through self-combustion method. *Journal of Advanced Dielectrics*. 2017;7(06):1750043.
6. Fernandes J, Guimarães R, Continentino M, Ziemath E, Walmsley L, Monteverde M, et al. Transport properties of the transverse charge-density-wave system  $\text{Fe}_3\text{O}_2\text{BO}_3$ . *Physical Review B*. 2005;72(7):075133.
7. Kumari K. Phase analysis, FTIR/Raman, and optical properties of  $\text{Fe}_3\text{BO}_6$  nanocrystallites prepared by glass route at moderate temperature in ambient air. *Journal of Molecular Structure*. 2018;1173:417-21.
8. Beutier G, Ovchinnikova E, Collins S, Dmitrienko V-E, Lorenzo J-E, Hodeau J-L, et al. Interplay of inequivalent atomic positions in resonant x-ray diffraction of  $\text{Fe}_3\text{BO}_6$ . *Journal of Physics: Condensed Matter*. 2009;21(26):265402.
9. Ibarra-Palos A, Darie C, Proux O, Hazemann J, Aldon L, Jumas J, et al. Electrochemical reactions of iron borates with lithium: Electrochemical and in situ Mössbauer and X-ray absorption studies. *Chemistry of materials*. 2002;14(3):1166-73.
10. Rowsell J, Gaubicher J, Nazar L. A new class of materials for lithium-ion batteries: iron (III) borates. *Journal of power sources*. 2001;97:254-7.
11. Tian J, Wang B, Zhao F, Ma X, Liu Y, Liu HK, et al. Highly active  $\text{Fe}_3\text{BO}_6$  as an anode material for sodium-ion batteries. *Chemical Communications*. 2017;53(34):4698-701.

12. Shi X, Chang C, Xiang J, Xiao Y, Yuan L, Sun J. Synthesis of nanospherical Fe<sub>3</sub>BO<sub>6</sub> anode material for lithium-ion battery by the rheological phase reaction method. *Journal of Solid State Chemistry*. 2008;181(9):2231-6.
13. Li S, Xu L, Zhai Y, Yu H. Co-pyrolysis synthesis of Fe<sub>3</sub>BO<sub>6</sub> nanorods as high-performance anodes for lithium-ion batteries. *RSC Advances*. 2014;4(16):8245-9.
14. Diehl R, Friedrich F. Growth of bulk single crystals of the weak ferromagnet Fe<sub>3</sub>BO<sub>6</sub> by a vapor phase reaction. *Journal of Crystal Growth*. 1976;36(2):263-6.
15. Kumari K. Structural, vibrational and surface analysis of Fe<sub>3</sub>BO<sub>6</sub> nanoplates synthesized by combustion method. *Journal of Molecular Structure*. 2018;1165:293-8.
16. Kumari K, Ram S, Kotnala R. Self-controlled growth of Fe<sub>3</sub>BO<sub>6</sub> crystallites in shape of nanorods from iron-borate glass of small templates. *Materials Chemistry and Physics*. 2011;129(3):1020-6.
17. Varma A, Mukasyan AS, Rogachev AS, Manukyan KV. Solution combustion synthesis of nanoscale materials. *Chemical reviews*. 2016;116(23):14493-586.
18. Baykan D, Oztas NA. Synthesis and characterization of iron orthophosphate by solution combustion method. *Materials Research Bulletin*. 2012;47(12):4013-6.
19. Miranda EAC, Carvajal JFM, Baena OJR. Effect of the fuels Glycine, urea and citric acid on the synthesis of the ceramic pigment ZnCr<sub>2</sub>O<sub>4</sub> by solution combustion. *Materials Research*. 2015;18(5):1038-43.
20. Ozdemir A, Altunal V, Kurt K, Depci T, Yu Y, Lawrence Y, et al. Thermoluminescence properties of Li<sub>2</sub>B<sub>4</sub>O<sub>7</sub>: Cu, B phosphor synthesized using solution combustion technique. *Radiation Physics and Chemistry*. 2017;141:352-62.
21. Palaspagar R, Gawande A, Sonekar R, Omanwar S. Fluorescence properties of Tb<sup>3+</sup> and Sm<sup>3+</sup> activated novel LiAl<sub>7</sub>B<sub>4</sub>O<sub>17</sub> host via solution combustion synthesis. *Materials Research Bulletin*. 2015;72:215-9.
22. Khan Z, Ingale N, Omanwar S. Synthesis and thermoluminescence properties of rare-earth-doped NaMgBO<sub>3</sub> phosphor. *Environmental Science and Pollution Research*. 2016;23(10):9295-302.
23. Pathak P, Kurchania R. Study of thermoluminescence properties of europium doped strontium borate phosphor exposed to Co-60 and photon beams (6 MV and 16 MV). *Physica B: Condensed Matter*. 2018.
24. Onani MO, Okil JO, Dejene FB. Solution-combustion synthesis and photoluminescence properties of YBO<sub>3</sub>: Tb<sup>3+</sup> phosphor powders. *Physica B: Condensed Matter*. 2014;439:133-6.
25. Altuntaş Öztaş N, Erdoğan H. Synthesis and characterization of magnesium pyroborate by solution combustion and conventional ceramic methods: A comparative study. *Zeitschrift für anorganische und Allgemeine Chemie*. 2009;635(11):1626-32.
26. Barpanda P, Yamashita Y, Chung S-C, Yamada Y, Nishimura S, Yamada A. Revisiting the Lithium Iron Borate (LiFeBO<sub>3</sub>) Cathode System: Synthetic and Electrochemical Findings. *ECS Transactions*. 2013;50(24):21-6.
27. Jain S, Adiga K, Verneker VP. A new approach to thermochemical calculations of condensed fuel-oxidizer mixtures. *Combustion and flame*. 1981;40:71-9.
28. Xu G, Li L, Shen Z, Tao Z, Zhang Y, Tian H, et al. Magnetite Fe<sub>3</sub>O<sub>4</sub> nanoparticles and hematite α-Fe<sub>2</sub>O<sub>3</sub> uniform oblique hexagonal microdisks, drum-like particles and spindles, and their magnetic properties. *Journal of Alloys and Compounds*. 2015;629:35-42.
29. Jiles D.C. *Introduction to Magnetism and Magnetic Materials*, ed. Chapman and Hall. 1998, New York.